J. Am. Soc. Mass Spectrom. (2011) 22:545–556
DOI: 10.1007/s13361-010-0059-7

RESEARCH ARTICLE

Differentiation of Isomeric Hydroxypyridine *N*-Oxides Using Metal Complexation and Electrospray Ionization Mass Spectrometry

Matias Butler,[1] Pau Arroyo Mañez,[2] Gabriela M. Cabrera[1]

[1]Departamento de Química Orgánica, UMyMFOR-CONICET, Facultad de Ciencias Exactas y Naturales, Universidad de Buenos Aires., Ciudad Universitaria Pabellón II, 3° piso, C1428EHA, Buenos Aires, Argentina
[2]Departamento de Química Inorgánica, Analítica, y Química Física, INQUIMAE-CONICET, Facultad de Ciencias Exactas y Naturales, Universidad de Buenos Aires, Ciudad Universitaria, Pabellón II, 1ºpiso, Buenos Aires, C1428EHA, Argentina

Abstract

Differentiation between two isomers of hydroxypyridine *N*-oxide according to the metal cation adducts generated by electrospray ionization (ESI) was investigated for different metal cations, namely Mg (II), Al (III), Ca (II), Sc (III), Fe (III), Co (II), Ni (II), Cu (II), Zn (II), Ga (III), besides the diatomic cation VO(IV). Protonated molecules of the isomeric hydroxypyridine *N*-oxides as well as the singly/doubly charged adducts formed from neutral or deprotonated ligands and a doubly/triply charged cation were produced in the gas phase using ESI, recording mass spectra with different metal ions for each isomer. While complex formation was successful for 2-hydroxypyridine *N*-oxide with trivalent ions, in the case of 3-hydroxypyridine *N*-oxide, only peaks related to the protonated molecule were present. On the other hand, divalent cations formed specific species for each isomer, giving characteristic spectra in every case. Hence, differentiation was possible irrespective of the metal cation utilized. In addition, quantum chemical calculations at the B3LYP/6-31+G(d,p) level of theory were performed in order to gain insight into the different complexation of calcium(II) with the isomers of hydroxypyridine *N*-oxide. The relative stability in the gas phase of the neutral complexes of calcium made up of two ligands, as well as the singly charged and doubly charged complexes, was investigated. The results of these calculations improved the understanding of the differences observed in the mass spectra obtained for each isomer.

Keywords: Electrospray, Metal complexation, Hydroxypyridine N-oxides

Introduction

The potential of electrospray ionization (ESI) for obtaining and studying gas-phase metal complexes was realized soon after the method had been introduced by Fenn and co-workers as a soft-ionization technique for polar involatile molecules [1]. Complexation with metal ions in solution, followed by efficient transport of charged complexes to the gas phase by ESI, represents a promising method for ionization of a variety of analytes, including those that are not directly amenable to ESI. Within the past decade, alkali, alkaline earth, and transition metal ions have been extensively used in ESI for many types of compounds. For example, metal ions have been successfully used for stereochemical differentiation by tandem mass spectrometry of some bicyclic diols [2] and glycosyl dithioacetals [3].

Electronic supplementary material The online version of this article (doi:10.1007/s13361-010-0059-7) contains supplementary material, which is available to authorized users.

Correspondence to: Gabriela M. Cabrera; *e-mail:* gabyc@qo.fcen.uba.ar

Received: 7 October 2010
Revised: 27 November 2010
Accepted: 29 November 2010
Published online: 1 February 2011

Moreover, transition and alkaline earth metals were used to differentiate isomeric flavonoids based on metal complexation and tandem mass spectrometry [4].

Differentiation of heterocyclic *N*-oxides and their isomeric hydroxylated metabolites is relevant since they are formed during metabolic biotransformation of many drugs. When *N*-oxidation or hydroxylation occurs on the same aromatic ring, tandem mass spectra obtained are usually very similar. For example, the similarity of the tandem mass spectra of protonated 8-hydroxyquinoline and quinoline *N*-oxide obtained by ESI showed that these isomeric oxygenated compounds were indistinguishable by this method [5]. In a previous work we have reported the differentiation of hydroxypyridine *N*-oxide isomers by analyzing the dissociation behavior in positive-ion mode atmospheric pressure mass spectrometry, employing ESI as well as atmospheric pressure chemical ionization (APCI) and atmospheric pressure photoionization (APPI) sources [6].

In the present work, we investigate the differentiation of hydroxypyridine *N*-oxide isomers generating adducts corresponding to these molecules (neutral or deprotonated) attached to metal cations by ESI. The selected isomers are 2-hydroxypyridine *N*-oxide **1** and 3-hydroxypyridine *N*-oxide **2** (Scheme 1). 2-hydroxypyridine *N*-oxide **1** exists as a tautomeric mixture of **1-a** and **1-b**, **1-a** being the main tautomer in solution and in the crystal state [7].

The chelating properties of 2-hydroxypyridine *N*-oxide **1**, behaving as a heterocyclic analog of hydroxamic acids, have been reported previously by potentiometric and spectrophotometric methods for several divalent and trivalent metals [8–10]. The present work extends the investigation to mass spectrometry, including the isomeric ligand 3-hydroxypyridine *N*-oxide **2** in order to gain complementary insights into the behavior of both isomers as metal complexating agents.

This study included, among others, the trivalent metal ions iron (III), gallium (III), and aluminum (III), which are of interest for their abilities to form stable complexes when associated with hydroxamates [11]. Scandium (III) was also included for comparative purposes as complexation studies with this trivalent ion are far less common [12]. Some other environmental divalent metal ions [magnesium (II), calcium (II), cobalt (II), nickel (II), copper (II), and zinc (II)] have also been involved in the present study. Due to the biological relevance of the complexes of 2-hydroxypyridine *N*-oxide **1** with Vanadyl (IV) as insulinomimetic compounds [13], this diatomic cation was studied too.

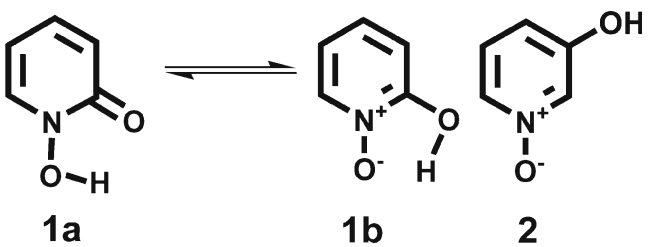

Scheme **1**. Structures of the *N*-oxides studied for isomer differentiation

In order to achieve a better understanding of the differences observed in the mass spectra of each isomer with metals, ab initio computational calculations were also performed. Characterization of the main ions obtained and analysis of the relative stability of the possible complexes formed in the gas phase may provide an important tool to understand the differences in the ion pattern of each isomeric hydroxypyridine *N*-oxide. The calcium complexes made up of two ligands of each isomer were chosen as a benchmark model. Such species were identified with MS (vide infra) for both isomers with important relative abundances, thus allowing direct comparisons between the experiment and theoretical calculations.

Experimental

Chemicals and Sample Preparation

2-Hydroxypyridine *N*-oxide and 3-hydroxypyridine *N*-oxide were purchased from Sigma-Aldrich (Milwaukee, WI, USA). LCMS grade methanol and HPLC grade water were purchased from Carlo Erba (Milan, Italy). The analyte solutions, each at a concentration of 10 mM, were prepared using methanol. The metal ion stock solutions, each at a concentration of 10 mM, were prepared using water from the metal salts of $MgCl_2$-$6H_2O$, $AlCl_3$, $CaCl_2$, $Sc(OTf)_3$, $VOSO_4$-$5H_2O$, $FeCl_3$-$6H_2O$, $CoCl_2$-$6H_2O$, $NiSO_4$-$7H_2O$, $CuSO_4$-$5H_2O$, $ZnCl_2$, and $GaCl_3$ obtained from Ga_2O_3 [14]. A small excess of HCl was added to the stock solutions of the trivalent metal ions.

Mass Spectrometry

Mass spectrometric analyses were performed using a Bruker micrOTOF-Q II mass spectrometer (Bruker Daltonics, Billerica, MA, USA), equipped with ESI. The instrument was operated at a capillary voltage of 4.5 kV with an end plate offset of –500 V, a dry temperature of 180 °C using N_2 as dry gas at 4.0 $l min^{-1}$ and a nebulizer pressure of 0.4 bar.

Multi-point mass calibration was carried out using a sodium formate solution from *m/z* 50 to 900 in positive ion mode. Data acquisition and processing were carried out using the Bruker Compass Data Analysis ver. 4.0 software supplied with the instrument.

The metal solutions in water were added in excess to solutions of each compound (approximately 2–3:1 ratios) prior to infusion into the mass spectrometer. Sample solutions were infused into the source using a KDS 100 syringe pump (KD Scientific, Holliston, MA, USA) at a flow rate of 180 $\mu L\ min^{-1}$.

Each experiment was repeated at least three times in different days in order to ensure reproducibility.

Computational Methods

All calculations were performed using the Gaussian 03 computational package [15]. Geometries of neutral, singly charged, and doubly charged molecules were optimized at

the B3LYP hybrid density functional level of theory (DFT) [16, 17] using the 6-31+G(d,p) basis set. This basis set, featuring both polarized and diffuse orbitals, has been proved to be well suited for investigating systems with delocalized charges [18]. The most probable protonation sites of the molecules were determined through analysis of the electrophilic Fukui function [19]. The optimized structures were characterized by harmonic frequency analysis as local minima (all frequencies real). Corrections for zero-point vibrational energy were included using the same level of theory.

Results and Discussion

Mass Spectrometry Study

Protonated molecules as well as metal cation adducts of the isomeric neutral or deprotonated hydroxypyridine *N*-oxides were produced in the gas phase using ESI. The solutions containing the different metals with each isomer were freshly prepared prior to infusion into the mass spectrometer recording their mass spectra after 5 min of infusion in order to let the stabilization of the species occur. The identity of the most significant metal cation adducts and their observed masses (with error in parenthesis) are listed in Tables 1 and 2 for isomers **1** and **2**, respectively. The confirmation of the assignments was based on high resolution mass-to-charge ratios, on collision induced dissociation (CID) product spectra and on analysis of the characteristic isotopic patterns of certain metals.

The key feature of mass spectra obtained with trivalent metal ions, except for scandium (vide infra), is the presence of a predominant specie for each isomer. The adduct made up of two deprotonated ligands attached to the metal cation dominated the spectra of isomer **1** (Figure 1), whereas only the peak arising from the protonated molecule was observed for isomer **2**. An analogous of the former adduct $[M + 2\ L - 2\ H]^+$ has been reported previously in ESI mass spectra of solutions of aluminum (III) with 2,3-dihydroxypyridine as ligand [20].

The relative stability of the diagnostic precursor ions $[M + 2\ L - 2\ H]^+$ obtained for isomer **1** was further investigated by CID. For this purpose, two approaches were employed: the determination of $E_{1/2}$ values [21] and CE_{50} values [22]. These parameters were extracted from the dissociation curves by plotting the relative abundance of the parent ion or the survival yield respectively, as a function of the collision energy corresponding to the lab frame, determining the value of the collision energy for 50% fraction or survival of the precursor ion. The estimated $E_{1/2}$ values obtained for the precursor ions $[M + 2\ L - 2\ H]^+$ of iron, aluminum and gallium are 16 eV, 23 eV, and 25 eV, respectively, while the CE_{50} values are 10 eV, 17.5 eV, and 20 eV, respectively. Therefore, both approaches are in very good agreement giving the same relative trend. The dissociation curves of the precursor ions $[M + 2\ L - 2\ H]^+$ are given in Supplementary Figures S1–S3 (see Supporting Information).

Table 1. Summary of the most significant[c] ions observed in the ESI mass spectra of isomer **1** (L) with metals (M); observed *m/z* (error in ppm). Values in bold indicate the most abundant ion for each metal. The largest peak of the isotope distribution is given

Ion/Metal M	^{24}Mg	^{27}Al	^{40}Ca	^{45}Sc	^{51}VO	^{56}Fe	^{59}Co	^{58}Ni	^{63}Cu	^{64}Zn	^{69}Ga
$[L+H]^+$								**112.0398** (4.2)			
$[M+L-H]^+$			149.9866 (2.1)		160.9680 (2.2)[b]		168.9568 (0.6)		172.9532 (0.4)	173.9527 (0.7)	
$[M+L+H_2O-H]^+$					178.9787 (3.1)[b]		**186.9674** (0.1)	185.9700 (2.3)	**190.9640** (0.7)	191.9634 (0.0)	
$[M+L+CH_3OH-H]^+$				335.9570 (2.5)[a]						205.9790 (0.4)	
$[M+L+2H_2O-H]^+$				339.9517 (3.1)[a]	196.9881 (3.5)[b]		204.9782 (1.1)		208.9743 (0.2)		
$[M+2L-H]^+$	245.0404 (1.2)		261.0178 (2.0)		271.9992 (1.5)[b]		279.9879 (3.4)	278.9903 (2.6)	283.9843 (3.5)	**284.9841** (2.4)	
$[M+2L-2H]^+$		247.0301 (3.0)			**286.9864** (1.2)	**275.9834** (2.1)					**288.9731** (1.0)
$[M+2L+H_2O-H]^+$	263.0507 (2.3)		279.0280 (3.1)		290.0096 (2.0)[b]						
$[M+2L+H_2O-2H]^+$						293.9934 (1.8)					
$[M+3L-H]^+$	**356.0723** (1.3)		**372.0486** (3.7)								
$[2M+3L-3H]^+$					**463.9507** (1.8)		447.9384 (0.1)		455.9313 (0.1)		

[a]Ions containing an additional triflate counter ion (X) actually observed. Also observed: 353.9675 (2.5) $[M+L+X+H_2O+CH_3OH-H]^+$ and 204.0088 (1.3) $[M+L+H_2O+CH_3OH-H]^+$
[b]Ions involving an oxygen atom loss actually observed
[c]Only ions with more than 25% relative intensities are listed

Table 2. Summary of the most significant[c] ions observed in the ESI mass spectra of isomer **2** (L) with metals (M); observed *m/z* (error in ppm). Values in bold indicate the most abundant ion for each metal. The largest peak of the isotope distribution is given

Ion/metal M/ counter ion X	^{24}Mg Cl	^{27}Al Cl	^{40}Ca Cl	^{45}Sc CF_3SO_3	^{51}VO SO_4	^{56}Fe Cl	^{59}Co Cl	^{58}Ni SO_4	^{63}Cu SO_4	^{64}Zn Cl	^{69}Ga Cl
$[L+H]^+$	112.0392 (1.0)	112.039 (1.7)	112.0394 (1.1)	112.0397 (3.8)	**112.0397** (3.2)	**112.0398** (4.1)	**112.0400** (6.2)	**112.0391** (2.2)	**112.0402** (8.1)	**112.0397** (3.8)	**112.0399** (5.1)
$[M+L+H_2O-H]^+$									191.9718 (0.7)[b]	191.9629 (2.4)	
$[M+L+X]^+$							204.9345 (4.7)			209.9304 (4.2)	
$[M+L+X+H_2O]^+$				471.9022 (0.3)[a]			**222.9448** (3.3)			227.9397 (1.4)	
$[M+2L]^+$									284.9925 (2.3)[b]		
$[M+2L+2H_2O]^{2+}$	141.0343 (1.6)		**149.0235** (0.9)								
$[M+2L+X]^+$				564.9225 (1.7)[a]			**315.9653** (0.8)			320.9607 (2.5)	
$[M+2L+H_2O+X]^+$	299.0263 (5.5)										
$[M+3L+H_2O]^{2+}$	**187.5450** (1.4)		195.5341 (0.1)				205.0195 (0.6)	204.5198 (3.4)			

[a]Ions containing an additional triflate counter ion (X) actually observed. Also observed: 353.9670 (3.9) $[M+L+X+H_2O+CH_3OH-H]^+$
[b]Ions containing Cu(I) species actually observed
[c]Only ions with more than 25% relative intensities are listed

Mass spectra obtained with divalent metal cations exhibited several characteristic species for each isomer. The main features of the mass spectra obtained with these ions are collected in Tables 1 and 2. The alkaline earth metal dications showed a slightly different behavior than the transition metal ions. This is illustrated in the mass spectra given in Figure 2, where calcium and copper were taken as examples. The complete mass spectra obtained with the other metal ions studied are shown in Supplementary Figures S4–S5 (see Supporting Information).

The main metal cation adducts observed for isomer **1** with alkaline earth metals were singly charged cations with up to three ligands including a water molecule. Unlike alkaline earth systems, transition metals with isomer **1** presented clusters with two metal centers and three ligands besides a major abundance of singly charged cations with up to two ligands including a water molecule.

It is remarkable that the assignments of the metal cation adducts of isomer **2** showed its ligands in their neutral form in spite of their similarity in stoichiometry to that observed with isomer **1**. In the case of alkaline earth metals, doubly charged adduct ions were predominant, while singly charged species with chloride attached were important for transition metals such as cobalt and zinc. This complexation behavior has been reported previously for metals such as calcium, magnesium, cobalt, and nickel, with a different monodentate ligand, namely 3-azidopropionitrile [23, 24]. As an exception, singly charged ions resulting from reduction of Cu (II) to Cu (I) were detected for isomer **2** in the case of copper, which is known to be easily reduced during the ESI process [25]. In the case of nickel, doubly charged species were detected corresponding to much less intense peaks compared to the protonated molecule of isomer **2**.

Vanadyl exhibited several singly charged metal adducts resulting from reduction (oxygen loss) or oxidation in the case of isomer **1**, whereas the protonated molecule was the only peak observed for isomer **2**. This behavior is in agreement with the variety of oxidation states attainable by vanadium [26].

Although scandium is a trivalent ion, the metal adduct ions displayed in its mass spectra were reminiscent of those observed with the divalent metal chloride systems, where the counter ion remains attached to the adduct. Moreover, the further incorporation of several molecules of solvent (i.e., water and methanol) rather complicated its mass spectra.

The differences observed between the isomers may be explained considering the ability of isomer **1** to form stable chelates acting as a bidentate ligand that limits the coordination of surrounding molecules in contrast to its isomer **2**.

Computational Study

Support was sought from theoretical calculations in order to bring some insights into the different complexation of 2-hydroxypyridine *N*-oxide **1** and 3-hydroxypyridine *N*-oxide

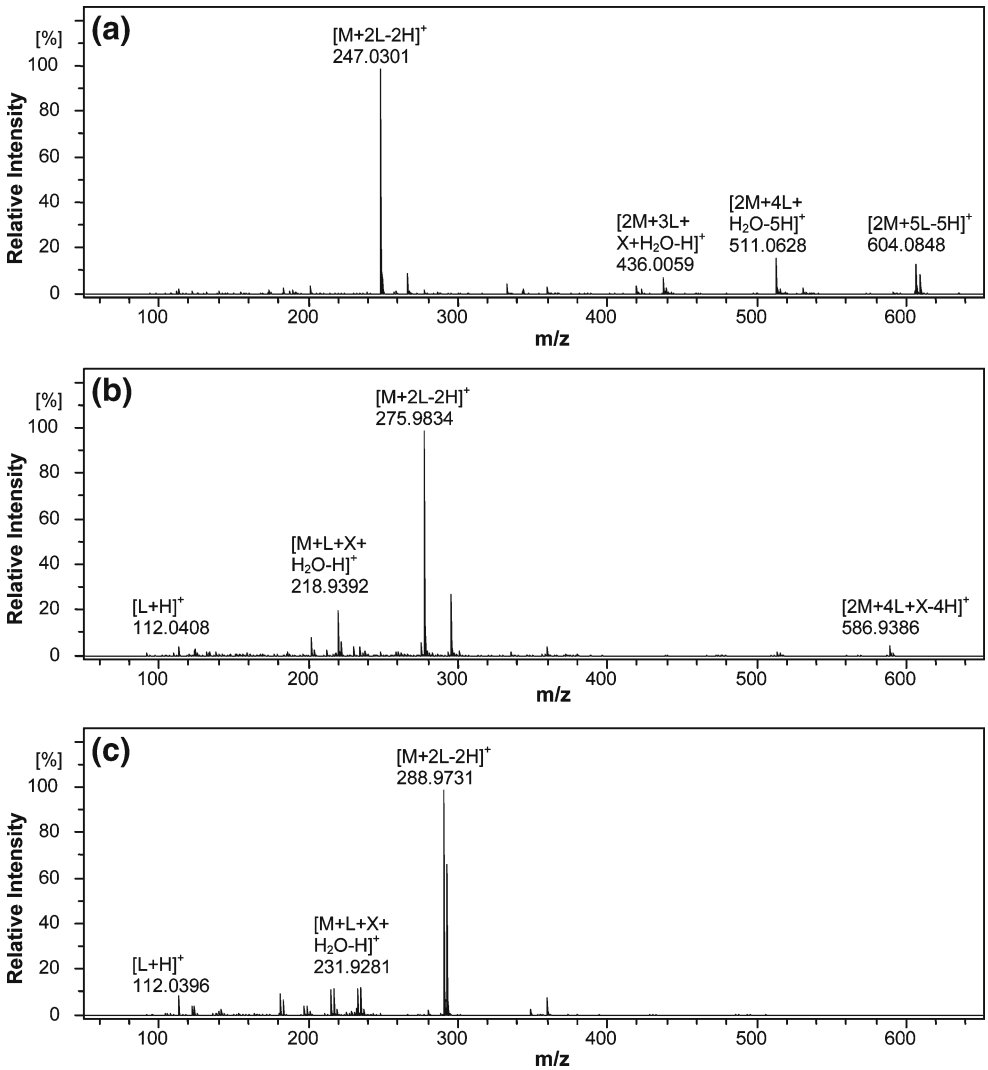

Figure 1. Representative mass spectra recorded for electrospray produced metal adducts of neutral/deprotonated 2-hydroxypyridine *N*-oxide **1** (L) with the trivalent metal ions (M): (**a**) aluminum; (**b**) iron; (**c**) gallium; with counter ion (X): chloride

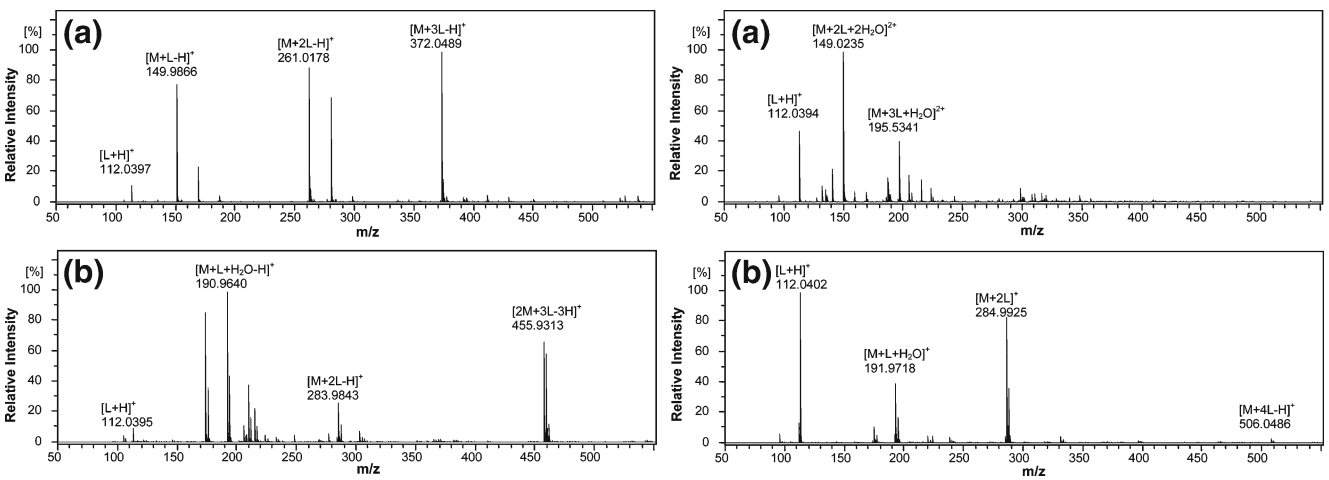

Figure 2. Representative mass spectra recorded for electrospray produced metal adducts of neutral/deprotonated hydroxypyridine *N*-oxides (L) **1** (left) and **2** (right) with the divalent metal ions (M): (**a**) calcium; (**b**) copper

2 with calcium (II). The *bis*-ligand stoichiometry was chosen for comparative reasons between both systems because of the relative abundance these species exhibited in the mass spectra (Figure 2a). Water molecules were excluded from the model in order to simplify it by reducing the degrees of freedom of the system. Despite their intervention in many complexes as seen in Tables 1 and 2, this simplification aimed to capture the essential features of the system.

The purpose of this study was to obtain a set of structures and energies of the possible neutral, singly charged, and doubly charged *bis*-ligand calcium complexes in order to ascertain the stability of the different species for each isomer. The neutral complexes were taken as a starting point to facilitate the succeeding calculations, as the charged complexes may be obtained by successive protonations.

Characterization of the relevant structures of the neutral complexes of calcium containing two deprotonated ligands of isomers **1** and **2** was carried out by exploratory ab initio calculations. Full geometry optimizations were performed obtaining the structures displayed in Figure 3. Frequency analysis of the stationary structures obtained was performed to complete the characterization. The prefixes I (N-*O*) and II (C-*O*) are used to indicate the oxygen atoms involved in the different coordination modes obtained for isomer **2**.

As it follows from Figure 3, two enantiomeric complexes **1C** were found for isomer **1**, containing the two ligands coordinated to the metal ion through both oxygen atoms forming a "tetrahedral-like" environment around calcium ion with a dihedral angle between the aromatic rings of 93°. Such unusual coordination has been reported recently for calcium caffeates [27]. On the other hand, extensive exploratory calculations on the complexes of isomer **2** revealed the inability of this ligand to behave as bidentate using both oxygen atoms. Instead, three different complexes were found, I,I'-**2C**; I,II'-**2C,** and II,II'-**2C**, presenting alternative coordination modes with the calcium cation bound to the two ligands through a single oxygen atom of each one (Figure 3).

Protonation Sites

The first step in the mass spectrum interpretation of ionized substances by protonation is the determination of the site in which this process occurs [28]. In this context, local reactivity indices such as the atomic nucleophilic indices (f_k^-), also known as electrophilic Fukui functions, provide an interesting alternative way to identify the most probable sites of protonation [19]. Recently, this methodology has been employed to identify the protonation sites in a series of natural and synthetic compounds [6, 29, 30].

In order to estimate the condensed Fukui function [31], two approaches were employed: the finite-difference approximation [32], using Mulliken population analysis (MPA) [33], and natural population analysis (NPA) [34] charges. The complete list of values is shown in Supplementary Table S1 (see Supporting Information). The most probable protonation sites obtained by the calculations depicted above are summarized in Table 3, showing that the oxygen atoms are the preferred protonation sites in all cases, differing in their identity according to the complex. It is significant that the most favored sites in the case of complexes formed with isomer **1**, are the oxygen atoms of the *N*-oxide moiety whereas for isomer **2** are the atoms non-coordinated to calcium.

It should be mentioned that in a previous work [6], we performed conformational studies of the protonated hydroxypyridine *N*-oxides **1** and **2** at the B3LYP/6-31++G(d,p) level of theory, finding two conformers for each isomer. In the stable conformations, the protonated oxygen group

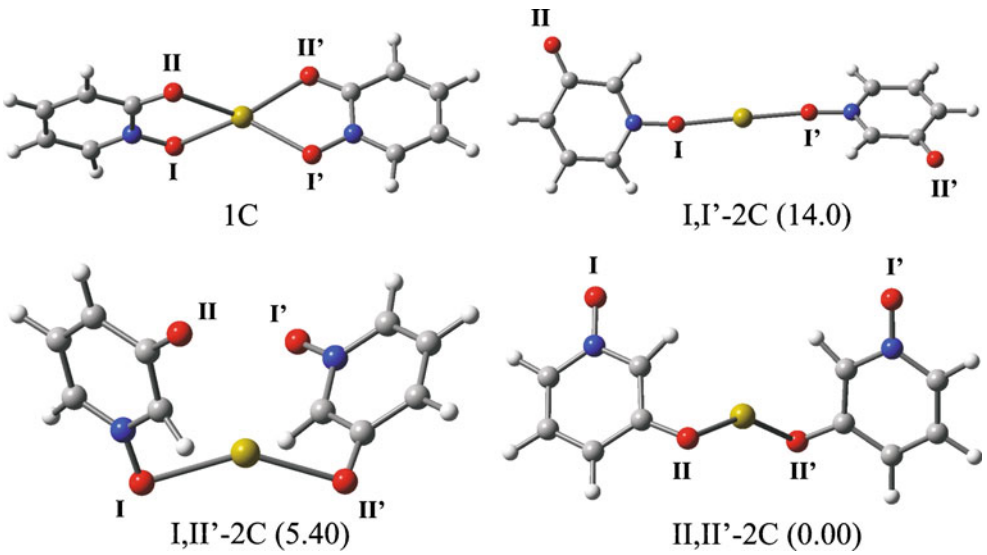

Figure 3. B3LYP/6-31+G(d,p) optimized geometries of the neutral *bis*-ligand calcium complexes of **1** and **2**. The values between brackets are the energy differences relative to the most stable complex of isomer **2** in kcal/mol (The most relevant optimum geometrical parameters of the structures are available in the Supporting Information)

Table 3. Summary of condensed Fukui functions for electrophilic attack for the *bis*-ligand neutral calcium complexes. Values in bold indicate the preferred site of protonation for each complex

Method site (k)	MPA f_k^-				NPA f_k^-			
	1C	I,I'–2C	I,II'–2C	II,II'–2C	1C	I,I'–2C	I,II'–2C	II,II'–2C
O(I)	**0.11**	0.02	0.05	**0.15**	**0.11**	0.02	0.05	**0.17**
O(II)	0.09	**0.14**	**0.13**	0.05	0.09	**0.16**	**0.15**	0.05
O(I')	**0.11**	0.02	**0.16**	**0.15**	**0.11**	0.02	**0.17**	**0.17**
O(II')	0.09	**0.14**	0.06	0.05	0.09	**0.16**	0.06	0.05

(hydroxyl) substituent was found to be coplanar with the aromatic ring, whereas the protonated oxygen group of the *N*-oxide moiety was oriented almost perpendicular to the aromatic ring, except when a hydrogen bond may occur in the structure, where was found to be coplanar. Hence, in all starting geometries of each one of the singly charged complexes, the initial conformations upon protonation were explored taking into account the afore-mentioned. The optimized structures of the stable conformations found for the singly charged complexes are shown in Figures 4 and 5. The suffixes I*H* (N-*O*) and II*H* (C-*O*) are used to indicate the identity of the protonated oxygen atom, while the different conformations corresponding to similar coordination modes and protonated atoms are distinguished by lowercase letters.

Protonation of **1C** according to the most favored positions (Table 3) led to three conformations: **1C**-I*H*a, **1C**-I*H*b, and **1C**-I*H*c (Figure 4). Moreover, protonation at the oxygen group substituent of the aromatic ring resulted in three additional conformations upon geometry optimizations calculated for comparative purposes: **1C**-II*H*a, **1C**-II*H*b, and **1C**-II*H*c (Figure 4). Six stable conformations were also found upon protonation of the different coordinated com-

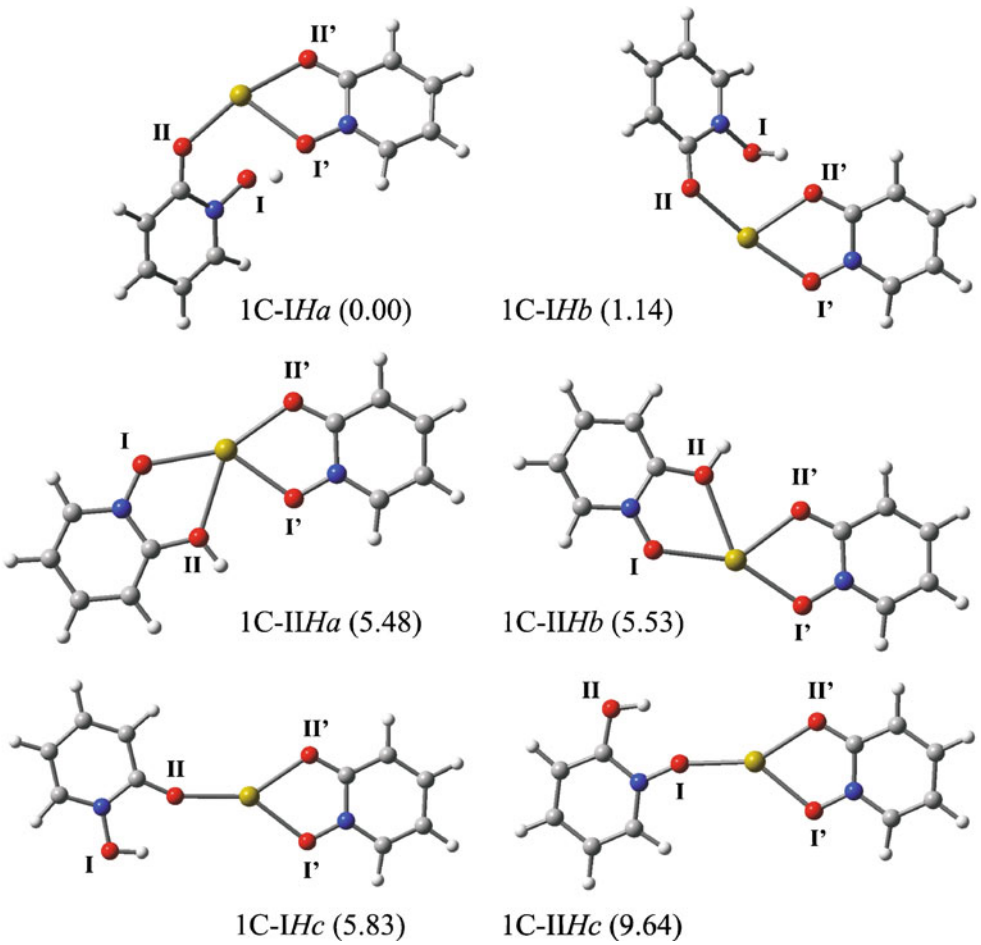

Figure 4. B3LYP/6-31+G(d,p) optimized geometries of the singly charged *bis*-ligand calcium complexes of **1**. The values between brackets are the energy differences relative to the most stable complex of the isomer in kcal/mol. (The most relevant optimum geometrical parameters of the structures are available in the Supporting Information)

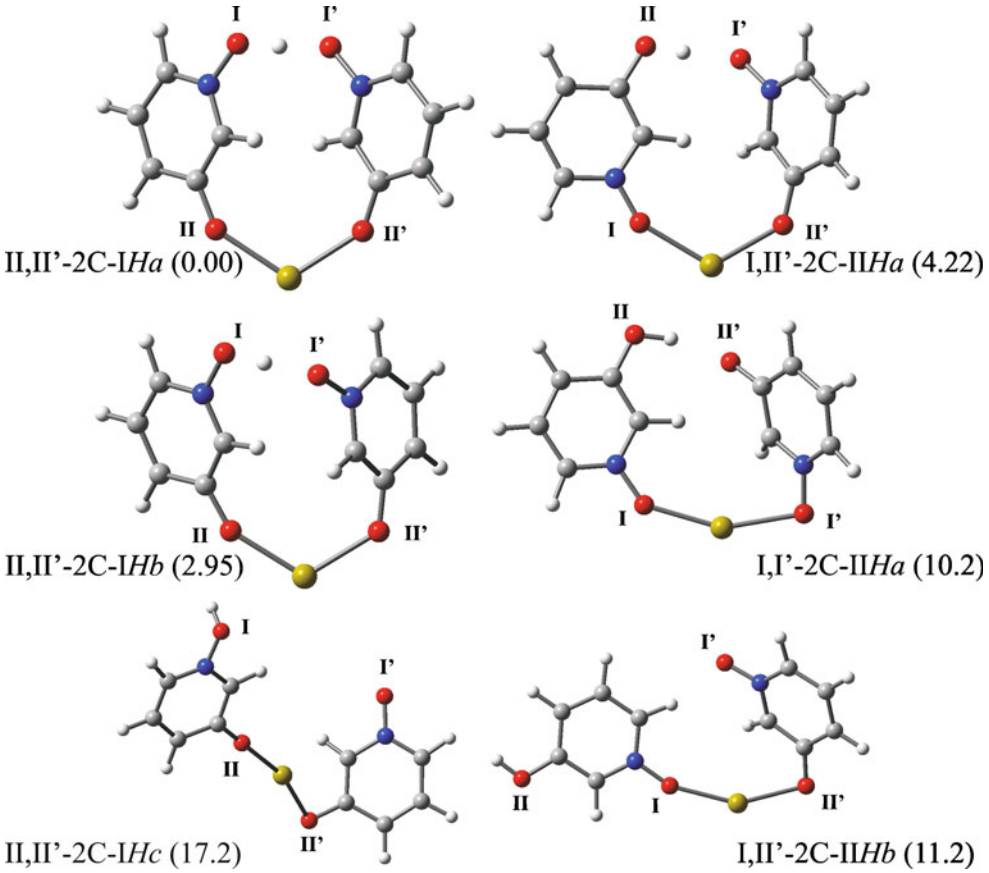

Figure 5. B3LYP/6-31+G(d,p) optimized geometries of the singly charged *bis*-ligand calcium complexes of **2**. The values between brackets are the energy differences relative to the most stable complex of the isomer in kcal/mol. (The most relevant optimum geometrical parameters of the structures are available in the Supporting Information)

plexes of **2C** according to the most favored positions: I,I'-**2C**-II*H*a, I,II'-**2C**-II*H*a, I,II'-**2C**-II*H*b, II,II'-**2C**-I*H*a, II,II'-**2C**-I*H*b, and II,II'-**2C**-I*H*c (Figure 5).

Upon analyzing the relative energy differences among the conformations found of the singly charged complexes of each isomer, it is interesting to note that the most stable ones correspond to geometries where the formation of a hydrogen bond involving both ligands is feasible (Figures 4 and 5). Concerning isomer 1 calcium complexes (Figure 4), two conformations with a hydrogen bond between the ligands were found (**1C**-I*H*a and **1C**-I*H*b). In the remaining conformations, both ligands were close to be coplanar, having either coordination number 4 and no hydrogen bonds (**1C**-II*H*a and **1C**-II*H*b) or coordination number 3 with an intramolecular hydrogen bond (**1C**-I*H*c and **1C**-II*H*c). On the other hand four conformations with intermolecular hydrogen bonds were found for calcium complexes of isomer **2** (I,I'-**2C**-II*H*a; I,II'-**2C**-II*H*a and II,II'-**2C**-I*H*a), besides II,II'-**2C**-I*H*b which resulted very similar and slightly more energetic than II,II'-**2C**-I*H*a (Figure 5). Conformations without hydrogen bonds (I,II'-**2C**-II*H*b and II,II'-**2C**-I*H*c) resulted to be more extended as expected from the absence of further stabilizing interactions between both ligands.

In the subsequent stage, the structures of the doubly charged complexes were optimized upon protonation, according to the most favored positions calculated, of certain structures in order to reduce the extent of calculations. Two distinctive structures were selected among the less energetic singly charged complexes of each isomer, namely **1C**-I*H*a and **1C**-I*H*b as well as I,II'-**2C**-II*H*a and II,II'-**2C**-I*H*a. The most probable protonation sites obtained in an analogous fashion to that depicted previously are summarized in Table 4 and once more the oxygen atoms are the preferred protonation sites and rather those belonging to the preceding non protonated ligand. The complete list of values is shown in Supplementary Table S2 (see Supporting Information). It is interesting to note that some carbon atoms belonging to the preceding non protonated ligand exhibit large values as well, although lower than the oxygens. This behavior may be attributed to the well known strong ortho- and para-directing effect of the hydroxyl or deprotonated hydroxyl moiety of enhancing the nucleophilic character at the ortho and para positions of the aromatic ring.

Different starting initial conformations were explored upon protonation (vide supra) but in this occasion, fewer conformations were found for each double positively

Table 4. Summary of condensed Fukui functions for electrophilic attack for the singly charged *bis*-ligand calcium complexes. Values in bold indicate the preferred protonation sites for each complex

Method	MPA f_k^-				NPA f_k^-			
Site (k)	1C–I*H*a	1C–I*H*b	I,II'-2C–II*H*a	II,II'-2C–I*H*a	1C–I*H*a	1C–I*H*b	I,II'–2C–II*H*a	II,II'–2C–I*H*a
O(I)	0.01	0.01	0.05	0.05	0.02	0.01	0.04	0.05
O(II)	0.06	0.05	0.01	0.07	0.06	0.04	0.01	0.08
O(I')	0.08	**0.17**	**0.22**	**0.12**	0.09	**0.18**	**0.24**	**0.13**
O(II')	**0.16**	0.13	0.12	**0.12**	**0.17**	0.14	0.13	**0.13**

charged complex obtained upon protonation of the corresponding singly charged cation. The most relevant structures are shown in Figure 6 and the remaining ones in Figure S6 (see Supporting Information). In respect of I,II'-**2C-**II*H*a, protonation at the oxygen group substituent of the aromatic ring resulted in an additional doubly charged cation calculated for comparative purposes.

It can be seen from Figure 6 that as regards the energy differences among the conformations found for the doubly charged complexes of each isomer, the most stable structures correspond to geometries where the formation of hydrogen bonds is no longer possible between both ligands. This behavior is contrary to that observed previously for the singly charged complexes. In connection with the conformations obtained, isomer **1** complexes display both ligands coplanar (**1C-**I,II'*H*a, **1C-**I,II'*H*b and **1C-**I,I'*H*a), whereas for isomer **2** complexes the dihedral angle between the aromatic rings of both ligands is about 90° (I,II'-**2C-**I',II*H*a, II,II'-**2C-**I, I'*H*a, and II,II'-**2C-**I,I'*H*b). In relation to isomer **2** complexes, the collinear extended conformations resulted less energetic than the more compacted ones (I,II'-**2C-**II,II'*H*a and II,II'-**2C-**I,II'*H*a) (see Supporting Information).

Ionized Complexes Stability

Once obtained the structures of the singly charged and doubly charged calcium complexes of each isomer, it remains to be seen if the analysis of their relative stability

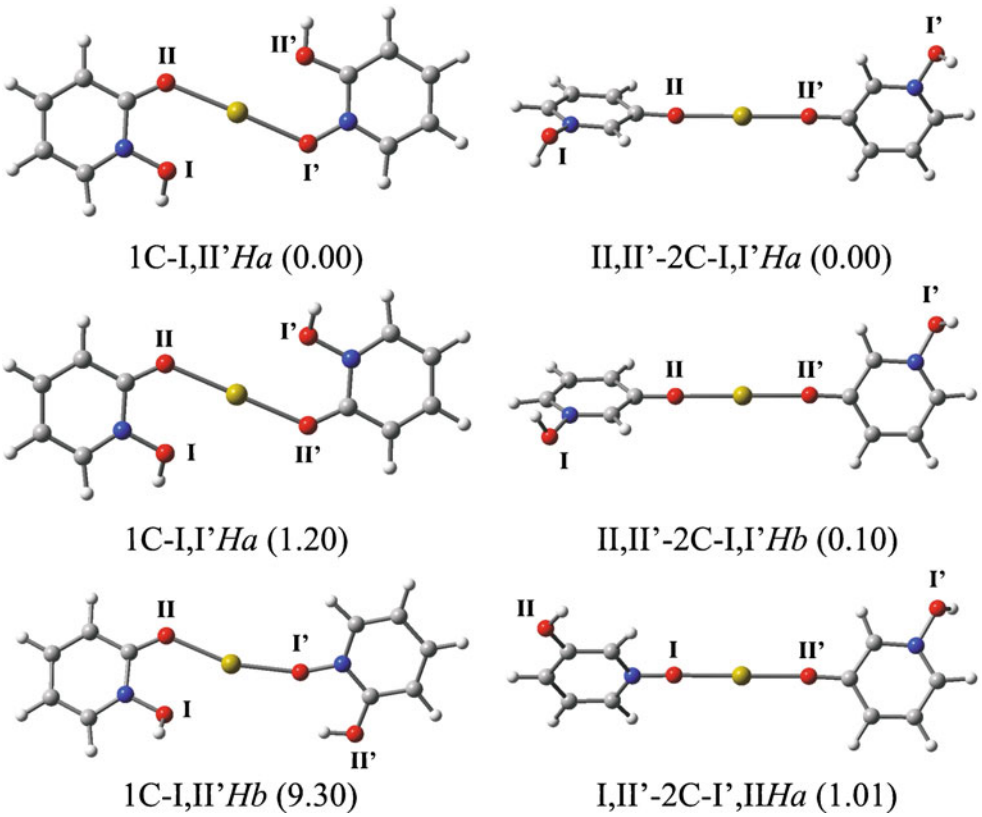

Figure 6. B3LYP/6-31+G(d,p) optimized geometries of the doubly charged *bis*-ligand calcium complexes of **1** and **2**. The values between brackets are the energy differences relative to the most stable complex of each isomer in kcal/mol. (The most relevant optimum geometrical parameters of the structures are available in the Supporting Information)

Table 5. Complexation energies (kcal mol^{-1}) for the singly charged *bis*-ligand calcium complexes

Complex	CE	Complex	CE
1C–1*Ha*	–29.9	I,I'-2C–II*Ha*	3.23
1C–1*Hb*	–28.8	II,I'-2C–II'*Ha*	–2.74
1C–1*Hc*	–24.1	II,I'-2C–II'*Hb*	4.19
1C–II*Ha*	–24.4	II,II'-2C–I*Ha*	–6.96
1C–II*Hb*	–24.4	II,II'-2C–I*Hb*	–4.01
1C–II*Hc*	–20.3	II,II'-2C–I*Hc*	10.2

CE = energy difference between the singly charged complex plus a proton and its two neutral ligands plus the calcium ion

explains the differences observed in the mass spectra recorded with calcium (Figure 2a).

Initially, the relative stability of the singly charged complexes plus a proton upon dissociation into its two neutral ligands and the calcium dication according to (1) was investigated. Complexation energies *CE* for the singly charged complexes (Table 5) were calculated from the following expression:

$$CE = \mathrm{E_C} - \mathrm{E_{Ca(II)}} - 2\,\mathrm{E_L}, \qquad (1)$$

where $\mathrm{E_C}$ is the calculated energy of the complex, $\mathrm{E_{Ca(II)}}$ that of isolated calcium dication, and $\mathrm{E_L}$ that of the most stable conformation of the corresponding neutral ligand.

It can be seen from Table 5 that the inherent higher stability of the complexes of **1** compared with that of **2** upon dissociation. Such stabilization is understandable in terms of the structures and coordination modes found in the complexes of each isomer (Figures 4 and 5). It is interesting to note that singly charged metal adducts were not observed in the corresponding mass spectra of isomer **2,** whereas they rank among the most important species observed in the case of isomer **1** (Figure 2a). Thus, calculated complexation energy values might account for the different relative intensities of the singly charged metal adducts in the mass spectra of each isomer.

Finally, relative stability of doubly charged species upon deprotonation by a neutral molecule generating two singly charged molecules was analyzed, i.e., (2), (3), (4). Possible relevant neutral molecules are the neutral complexes as well as the solvent molecules present in the source, namely methanol and water. Deprotonation energy values were calculated for the different complexes found for each isomer, where dE_1 is the energy difference between the neutral precursor and its singly charged complex and dE_2 is the energy difference between the singly charged precursor and its doubly charged complex (Table 6).

Stability is related to the deprotonation energy differences according to the following equations:

$$[\mathrm{CaL_2}]^{++} + [\mathrm{CaL_2} - 2\mathrm{H}] \rightleftarrows 2[\mathrm{CaL_2} - \mathrm{H}]^{+} \qquad (2)$$
$$\mathrm{dE} = dE_2 - dE_1$$

$$[\mathrm{CaL_2}]^{++} + \mathrm{H_2O} \rightleftarrows [\mathrm{CaL_2} - \mathrm{H}]^{+} + \mathrm{H_3O}^{+} \qquad (3)$$
$$\mathrm{dE} = dE_2 - dE_{H2O}$$

$$[\mathrm{CaL_2}]^{++} + \mathrm{CH_3OH} \rightleftarrows [\mathrm{CaL_2} - \mathrm{H}]^{+} + \mathrm{CH_3OH_2}^{+} \qquad (4)$$
$$\mathrm{dE} = dE_2 - dE_{CH3OH}$$

Taking together the values of Table 6 and (2), the conclusion can be drawn that in all cases, $dE_1 > dE_2$, thus indicating the incompatibility of diprotonated and neutral species as expected. However, in the absence of neutral complexes, surrounding solvent molecules must be taken into consideration. The literature values [35] for the proton affinities of water and methanol are 165.2 kcal mol^{-1} and 180.3 kcal mol^{-1}, respectively. In an analogous fashion to that employed in Table 6, the deprotonation energies of the oxonium ions of water and methanol were calculated giving values of 163.6 kcal mol^{-1} and 179.1 kcal mol^{-1}, respectively. Therefore, the good agreement between the calculated values (energies at 0 K) and the literature values (enthalpies at 298 K) provides support to the model used for the calculations in which the effect of the thermal and enthalpic corrections cancel when the energy difference is calculated as observed in the cases studied. However, the translational enthalpy of proton (5/2*RT*) is the most important thermal contribution (1.5 kcal mol^{-1}) [36] and its neglect probably might account for the systematic lower value of the energies calculated compared with the proton affinities.

Comparing the values obtained for the solvent molecules with those reported in Table 6 (dE_2) for the most stable

Table 6. Deprotonation energies (kcal mol^{-1}) for the singly charged and doubly charged *bis*-ligand calcium complexes

Complex	dE_1	Complex	dE_1	Complex	dE_2	Complex	dE_2
1C–1*Ha*	219.9	I,I'–2C-II*Ha*	259.1	1C–I,II'*Ha*	146.1	I,II'–2C–I',II*Ha*	182.3
1C–1*Hb*	218.7	I,II'–2C-II*Ha*	256.4	1C–I,II'*Hb*	136.8	I,II'–2C–II,II'*Ha*	142.5
1C–1*Hc*	214.1	I,II'–2C-II*Hb*	249.5	1C–I,I'*Ha*	146.1	II,II'–2C–I,II'*Ha*	139.5
1C–II*Ha*	214.4	II,II'–2C-I*Ha*	255.3			II,II'–2C–I,I'*Ha*	179.1
1C–II*Hb*	214.4	II,II'–2C-I*Hb*	252.3			II,II'–2C–I,I'*Hb*	179.0
1C–II*Hc*	210.2	II,I'–2C-I*Hc*	238.1				

dE_1: energy difference between the neutral precursor and its singly charged complex
dE_2: energy difference between the singly charged precursor and its doubly charged complex

complexes of each isomer, it can be seen that doubly charged complexes of **2** are stable upon deprotonation by solvent (dE > 0) while those of **1** are not (3), (4). These results suggest a reasonable explanation for the different charged species observed in the mass spectra of both isomers, i.e., doubly charged species are the most important among the calcium complexes of **2** while they are not observed for **1** (Figure 2a).

Conclusions

Differentiation via metal complexation in positive ion mode electrospray mass spectrometry of two representative hydroxypyridine *N*-oxide isomers was investigated. In addition to the observation of singly charged metal adducts arising from one or two deprotonated ligands of 2-hydroxypyridine *N*-oxide **1** with divalent or trivalent metals, respectively, the presence of the ligands of 3-hydroxypyridine *N*-oxide **2** in their neutral form was noted in the doubly or singly charged metal adducts obtained with divalent metals besides its omnipresent protonated molecule. Both isomers could easily be distinguished, no matter the metal ion utilized, by comparing the characteristic ions exhibited in their mass spectra.

The relative stability of the *bis*-ligand isomeric hydroxypyridine *N*-oxide calcium complexes could be analyzed upon structural optimization of singly charged and doubly charged complexes using B3LYP/6-31+G(d,p). Quantum chemical calculations at the former level of theory suggest that the ability of isomer **1** of forming stable chelates acting as a bidentate ligand would stabilize the formation of singly charged species due to the presence of intermolecular hydrogen bonds. However, hydrogen bonds are lost upon formation of doubly charged species. Furthermore, these species are unstable as they might be deprotonated by solvent molecules. On the contrary, isomer **2** behaves as a monodentate ligand and only a slight energy difference exists between its proton bound complexes and the dissociated neutral ligands and calcium, thus showing an unfavorable formation of singly charged species. On the other hand, the most stable doubly charged species show stability upon deprotonation by solvent molecules as well. As a result, it could be suggested a reasonable rationalization for the observation of singly charged and doubly charged species as the most important *bis*-ligand calcium complexes of **1** and **2**, respectively.

Our results suggest that the characterization of the main metal adduct ions obtained as well as the analysis of the relative stability in the gas phase of the possible complexes formed with each isomer provide an important tool to achieve a better understanding of the differences observed in the mass spectra of both hydroxypyridine *N*-oxide isomers with metal cations. We conclude that it might be possible to explain and predict the mass spectrometric behavior of similar isomeric systems with metal cations in an analogous fashion.

Acknowledgements

The authors thank Universidad de Buenos Aires, CONICET and ANPCyT for financial support and CONICET for the fellowships to M.B. and P.A.M. Calculations were performed in Centro de Computos de Alto Rendimiento (CeCar) at Facultad de Ciencias Exactas y Naturales (FCEN) of Universidad de Buenos Aires. Cristián Huck Iriart is thanked for the donation of Ga_2O_3.

References

1. Turecek, F., Gatlin, C.L.: Electrospray ionization of inorganic and organometallic complexes. In: Cole, R.B. (ed.) Electrospray Ionization Mass Spectrometry: Fundamentals, Instrumentation, and Applications, p. 527. Wiley, New York (1997)
2. Pakarinen, J.M.H., Vainiotalo, P.: Diastereochemical differentiation of bicyclic diols using metal complexation and collision-induced dissociation mass spectrometry. *Rapid Commun. Mass Spectrom.* **23**, 1767–1775 (2009)
3. Madhusudanan, K.P., Kumar, B., Tiwari, P., Madhusudan, S.K., Misra, A.K.: Tandem mass spectra of transition-metal ion adducts of glycosyl dithioacetals; distinction among stereoisomers. *Rapid Commun. Mass Spectrom.* **19**, 470–476 (2005)
4. Davis, B.D., Brodbelt, J.S.: Determination of the glycosylation site of flavonoid monoglucosides by metal complexation and tandem mass spectrometry. *J. Am. Soc. Mass Spectrom.* **15**, 1287–1299 (2004)
5. Peiris, D.M., Lam, W., Michael, S., Ramanathan, R.: Distinguishing N-oxide and hydroxyl compounds: impact of heated capillary/heated ion transfer tube in inducing atmospheric pressure ionization source decompositions. *J. Mass Spectrom.* **39**, 600–606 (2004)
6. Butler, M., Arroyo Mañez, P., Cabrera, G.M.: An experimental and computational study on the dissociation behavior of hydroxypyridine N-oxides in atmospheric pressure ionization mass spectrometry. *J. Mass Spectrom.* **45**, 536–544 (2010)
7. Ballesteros, P., Claramunt, R.M., Cañada, T., Foces-Foces, C., Cano, F. H., Elguero, J., Fruchier, A.: A 1 H and 13 C nuclear magnetic resonance and X-ray diffraction study of the tautomerism of 2-hydroxy- and 2,3-dihydroxy-pyridine N-oxides. X-ray molecular structure of 2-hydroxypyridine N-oxide. *J. Chem. Soc. Perkin Trans. 2* **7**, 1215–1219 (1990)
8. Sun, P.J., Fernando, Q., Freiser, H.: Structure and behavior of organic analytical reagents formation constants of transition metal complexes of 2-hydroxypyridine-1-oxide and 2-mercaptopyridine-1-oxide. *Anal. Chem.* **36**, 2485–2486 (1964)
9. Farkas, E., Enyedy, E.A., Csóka, H.: Some factors affecting metal ion-monohydroxamate interactions in aqueous solution. *J. Inorg. Biochem.* **79**, 205–211 (2000)
10. Yue, J.-L., Martell, A.E.: Potentiometric and spectrophotometric determination of stabilities of the 1-hydroxy-2-pyridinone complexes of trivalent and divalent metal ions. *Inorg. Chim. Acta* **214**, 103–111 (1993)
11. Evers, A., Hancock, R.D., Martell, A.E., Motekaitis, R.J.: Metal ion recognition in ligands with negatively charged oxygen donor groups. Complexation of Fe(III), Ga(III), In(III), Al(III), and other highly charged metal ions. *Inorg. Chem.* **28**, 2189–2195 (1989)
12. Monfardini, I., Massi, L., Tremel, P., Hauville, A., Olivero, S., Duñach, E., Gal, J.-F.: Mass spectrometric characterization of metal triflates and triflimides (Lewis superacid catalysts) by electrospray ionization and tandem mass spectrometry. *Rapid Commun. Mass Spectrom.* **24**, 2611–2619 (2010)
13. Kiss, E., Kawabe, K., Tamura, A., Jakusch, T., Sakurai, H., Kiss, T.: Chemical speciation of insulinomimetic VO(IV) complexes of pyridine-N-oxide derivatives: binary and ternary systems. *J. Inorg. Biochem.* **95**, 69–76 (2003)
14. Brauer, G.: Handbook of Preparative Inorganic Chemistry, 2nd edn, p. 843. Academic Press, New York (1996)
15. Frisch, M.J., Trucks, G.W., Schlegel, H.B., Scuseria, G.E., Robb, M.A., Cheeseman, J.R., Montgomery Jr., J.A., Vreven, T., Kudin, K.N., Burant, J.C., Millam, J.M., Iyengar, S.S., Tomasi, J., Barone, V., Mennucci, B., Cossi, M., Scalmani, G., Rega, N., Petersson, G.A., Nakatsuji, H., Hada, M., Ehara, M., Toyota, K., Fukuda, R., Hasegawa, J., Ishida, M., Nakajima, T., Honda, Y., Kitao, O., Nakai, H., Klene, M., Li, X., Knox, J.E., Hratchian, H.P., Cross, J.B., Bakken, V., Adamo, C.,

Jaramillo, J., Gomperts, R., Stratmann, R.E., Yazyev, O., Austin, A.J., Cammi, R., Pomelli, C., Ochterski, J.W., Ayala, P.Y., Morokuma, K., Voth, G.A., Salvador, P., Dannenberg, J.J., Zakrzewski, V.G., Dapprich, S., Daniels, A.D., Strain, M.C., Farkas, O., Malick, D.K., Rabuck, A.D., Raghavachari, K., Foresman, J.B., Ortiz, J.V., Cui, Q., Baboul, A.G., Clifford, S., Cioslowski, J., Stefanov, B.B., Liu, G., Liashenko, A., Piskorz, P., Komaromi, I., Martin, R.L., Fox, D.J., Keith, T., Al-Laham, M.A., Peng, C.Y., Nanayakkara, A., Challacombe, M., Gill, P.M.W., Johnson, B., Chen, W., Wong, M.W., Gonzalez, C., Pople, J.A.: Gaussian 03, Revision C. 02. Gaussian, Inc, Wallingford (2004)

16. Lee, C., Yang, W., Parr, R.G.: Development of the Colle-Salvetti correlation-energy formula into a functional of the electron density. *Phys. Rev. B* **37**, 785–789 (1988)
17. Becke, A.D.: Density-functional thermochemistry. III. The role of exact exchange. *J. Chem. Phys.* **98**, 5648–5652 (1993)
18. El-Nahas, A.M., Hirao, K.: A theoretical study on 2-hydroxypyrazine and 2, 3-dihydroxypyrazine: tautomerism, intramolecular hydrogen bond, solvent effects. *J. Theochem* **459**, 229–237 (1999)
19. Fuentealba, P., Pérez, P., Contreras, R.: On the condensed Fukui function. *J. Chem. Phys* **113**, 2544–2551 (2000)
20. Di Marco, V.B., Ranaldo, M., Bombi, G.G., Traldi, P.: Surface-activated chemical ionization versus electrospray ionization in the study of selected aluminium(III)/ligand solution equilibria. *Rapid Commun. Mass Spectrom.* **20**, 710–712 (2006)
21. David, W.M., Brodbelt, J.S.: Threshold dissociation energies of protonated amine/polyether complexes in a quadrupole ion trap. *J. Am. Soc. Mass Spectrom.* **14**, 383–392 (2003)
22. Kertesz, T.M., Hall, L.H., Hill, D.W., Grant, D.F.: CE50: quantifying collision induced dissociation energy for small molecule characterization and identification. *J. Am. Soc. Mass Spectrom.* **20**, 1759–1767 (2009)
23. Henderson, W., McIndoe, J.S.: In: Mass Spectrometry of Inorganic, Coordination, and Organometallic Compounds, p. 117, 1st ed. John Wiley, Chichester (2005)
24. Couto, N., Ramos, M.J., Fernandez, M.T., Rodrigues, P., Barros, M.T., Costa, M.L., Cabral, B.J.C., Duarte, M.F.: Study of doubly charged alkaline earth metal and 3-azidopropionitrile complexes by electrospray ionization mass spectrometry. *Rapid Commun. Mass Spectrom.* **22**, 582–590 (2008)
25. Couto, N., Duarte, M.F., Fernandez, M.T., Rodrigues, P., Barros, M.T., Costa, M.L., Costa Cabral, B.J.: Complexation of transition metals by 3-Azidopropionitrile. An electrospray ionization mass spectrometry study. *J. Am. Soc. Mass Spectrom.* **18**, 453–465 (2007)
26. Buglyó, P., Pótári, N.: Study of the interaction between oxovanadium (IV) and hydroxamic acids. *Polyhedron* **24**, 837–845 (2005)
27. Maciejewska, G., Zierkiewicz, W., Adach, A., Kopacz, M., Zapała, I., Bulik, I., Cieślak-Golonka, M., Grabowski, T., Wietrzyk, J.: Atypical calcium coordination number: physicochemical study, cytotoxicity, DFT calculations, and in silico pharmacokinetic characteristics of calcium caffeates. *J. Inorg. Biochem.* **103**, 1189–1195 (2009)
28. Vessecchi, R., Galembeck, S.E., Lopes, N.P., Nascimento, P.G.B.D., Crotti, A.E.M.: Application of computational quantum chemistry to chemical processes involved in mass spectrometry [Aplicação da química quântica computacional no estudo de processos químicos envolvidos em espectrometria de massas]. *Quim. Nova* **31**, 840–853 (2008)
29. Cardozo, K.H.M., Vessecchi, R., Carvalho, V.M., Pinto, E., Gates, P.J., Colepicolo, P., Galembeck, S.E., Lopes, N.P.: A theoretical and mass spectrometry study of the fragmentation of mycosporine-like amino acids. *Int. J. Mass Spectrom.* **273**, 11–19 (2008)
30. Crotti, A.E.M., Bronze-Uhle, E.S., Nascimento, P.G.B.D., Donate, P. M., Galembeck, S.E., Vessecchi, R., Lopes, N.P.: Gas-phase fragmentation of γ-lactone derivatives by electrospray ionization tandem mass spectrometry. *J. Mass Spectrom.* **44**, 1733–1741 (2009)
31. Contreras, R.R., Fuentealba, P., Galván, M., Pérez, P.: A direct evaluation of regional Fukui functions in molecules. *Chem. Phys. Lett.* **304**, 405–413 (1999)
32. Yang, W., Mortier, W.J.: The use of global and local molecular parameters for the analysis of the gas-phase basicity of amines. *J. Am. Chem. Soc.* **108**, 5708–5711 (1986)
33. Mulliken, R.S.: Electronic population analysis on LCAO-MO molecular wave functions. I. *J. Chem. Phys.* **23**, 1833–1840 (1955)
34. Reed, A.E., Curtiss, L.A., Weinhold, F.: Intermolecular interactions from a natural bond orbital, donor-acceptor viewpoint. *Chem. Rev.* **88**, 899–926 (1988)
35. Hunter, E.P., Lias, S.G.: Evaluated gas phase basicities and proton affinities of molecules: an update. *J. Phys. Chem. Ref. Data* **27**, 413–656 (1998)
36. Czakó, G., Mátyus, E., Simmonett, A.C., Császár, A.G., Schaefer III, H. F., Allen, W.D.: Anchoring the absolute proton affinity scale. *J. Chem. Theory Comput.* **4**, 1220–1229 (2008)